euspen's 22nd International Conference & Exhibition, Geneva, CH, May/June 2022
www.euspen.eu

Uncertainty-based comparison of the effect of the area shape function on material characterisation in nanoindentation testing

Giacomo Maculotti[1], Gianfranco Genta[1], Andrea Carbonatto[1], Maurizio Galetto[1]

[1]*Department of Management and Production Engineering, Politecnico di Torino, Italy*

giacomo.maculotti@polito.it

Abstract

Instrumented Indentation Test (IIT) is largely exploited in industry and academia to achieve multi-scale mechanical characterisation, i.e. ranging from nano- and micro-structure to bulk, of several properties, e.g. Young's modulus, stress-strain curve, creep, and relaxation. IIT is particularly suited to cope with the challenges of the current industrial framework to achieve multi-objective characterisation and requirements of zero-defect manufacturing and zero waste. In fact, IIT requires limited sample preparation and is a non-destructive technique with high throughput. IIT consists of applying a loading-unloading force cycle on the specimen. The capability of continuously measuring the indenter displacement in the material, i.e. being a depth-sensing technique, is the essential feature of IIT. This allows the mechanical characterisation by knowing the shape of the indenter and hence the relationship between the indentation depth and the projected area of the surface in contact between the indenter and the specimen. The relationship is described by the area shape function, whose parameters require calibration according to ISO 14577-2:2015. For a given indenter geometry, several alternative models are available in the literature. These describe both the geometry and the possible presence of errors, e.g. blunt tip and wear effect. However, a comparison of the choice of the different alternatives, when they are equally nominally applicable, is lacking in the literature, although it prescribes some applicability ranges. This work exploits a simulative approach based on bootstrap sampling to estimate the uncertainty of the calibration of area shape function parameters in the nano-range, where the effect is critical. The uncertainty is then propagated to compare performances of different area shape function models on the mechanical characterisation, i.e. indentation hardness and Young's modulus estimate, within a rigorous metrological framework. Results are shown for standard reference materials, i.e. SiO_2 and W, to ensure proper composition homogeneity and neglect edge effects, i.e. pile-up and sink-in.

Keywords: Instrumented Indentation Test, Area shape function, Measurement Uncertainty, Bootstrap

1. Introduction

Instrumented Indentation Test (IIT) is a depth-sensing mechanical characterisation technique [1,2]. It is considered a non-conventional indentation testing technique, that provides a quick and non-destructive method to characterise materials' mechanical properties thoroughly. It consists in applying a loading-holding-unloading force, *F*, cycle to a test material. The force transducer present in the indentation platform, typically a piezoelectric or a three-plate capacitive transducer [3], measures the penetration depth *h*, i.e. the displacement of the indenter's tip in the material, throughout the whole indentation cycle. This results in the indentation curve (IC), F(h); an example is shown in Figure 1.

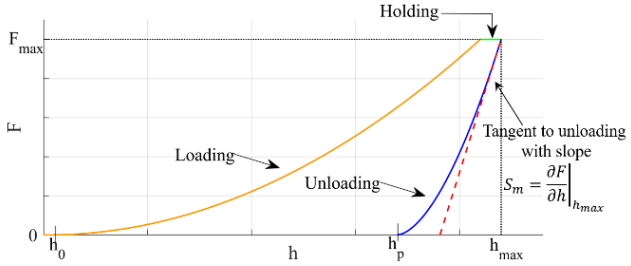

Figure 1. Example of IC showing relevant parameters.

The IC coupled with the knowledge of the area shape function $A_p=f(h;\ \boldsymbol{a})$, i.e. the mathematical relationship between *h* and the area of the projected contact surface between the indenter and sample A_p, allows overcoming limits inherent with optical systems, due to their resolution, and achieving multi-scale characterisation from bulk to nano scales [1,2]. In fact, IIT thanks to the IC and the $A_p=f(h)$ does not resolve the dimension of the indentation optically, differently from conventional hardness testing procedures, e.g. Vickers hardness. The functional form of $A_p=f(h;\ \boldsymbol{a})$ depends on the indenter geometry and the parameters $\boldsymbol{a}$ requires calibration [4,5]. Moreover, the analysis of the IC enables the characterisation of several mechanical properties in addition to the indentation hardness H_{IT}. Some examples are: the indentation moduls E_{IT}, i.e. an estimate of the Young's modulus, creep and relaxation properties [1,2,6], estimates of the plastic stress-strain curve [7], residual stresses [8]. Thus, IIT finds application in characterising mechanical properties [9,10] and characteristic dimensions [11] of the microstructure and thin and multi-layer coatings [12,13]. The related standard ISO 14577-1:2015 describes the characterisation procedure of more conventional quantities, i.e. H_{IT} and E_{IT}. This requires, first, to correct the measured displacement *h* from measurement errors that include: zero error, h_0, the elastic deformation of the machine, $C_f \cdot F$, and of the sample, $\varepsilon \cdot F/S$, which depends on the geometry of the indenter by the factor ε:

$$h_c = h - h_0 - \varepsilon \frac{F}{S} - C_f F \qquad (1).$$

Then, the analysis of the IC requires to evaluate the residual indentation h_p and the contact stiffness S_m, from which, knowing from calibration the frame compliance C_f the sample stiffness, *S*, results:

$$C_{tot} = \frac{1}{S_m} = \left(\left.\frac{\partial F}{\partial h}\right|_{h_{max}}\right)^{-1} = C_f + \frac{1}{S} \quad (2.1)$$

$$S = \left.\frac{\partial F}{\partial h_c}\right|_{h_{c,max}} \quad (2.2),$$

with C_{tot} being the total system compliance. S_m evaluation is critical [14] and can be performed according to several methodologies [15]. The standard [6] power-law method (PL) fits the unloading curve to the model $F = B(h - h_p)^m$ [16]. B depends on the tested material, m on indenter geometry, h_p is the residual indentation depth, and they are all obtained by non-linear regression. S_m is computed by differentiating the model and computing the derivative in the point corresponding to the onset of unloading.

Finally, the mechanical characterisation can be achieved as:

$$H_{IT} = \frac{F_{max}}{A_p(h_{c,max})} \quad (3.1)$$

$$E_{IT} = \frac{1 - \nu_s^2}{\frac{2\sqrt{A_p(h_{c,max})}}{S\sqrt{\pi}} - \frac{1 - \nu_i^2}{E_i}} \quad (3.2),$$

catering for the mechanical properties of the indenter, i.e. its Poisson's, ν_i, and Young's modulus, E_i, and the Poisson's modulus of the tested material, ν_s.

The literature [17] showed that major factors influencing the uncertainty are the stiffness of the platform and the parameters of A_p, i.e. C_f and $\boldsymbol{a}$, which need calibration. This is performed according to ISO 14577-2:2015, which presents some criticalities [18]. Amongst the others, the effect of the functional form of A_p on the metrological performances of the characterisation are unreported. Although the literature suggests some practical guidelines to choose the adequate model [4,6], thorough metrological assessment is lacking. This work performs a comparison within a metrological framework of the alternative area shape function functional forms. In detail, Section 2 presents the applied methodology, Section 3 discusses the results and Section 4 concludes on the findings.

2. Methodology

This work compares the effect of different area shape function models on the characterisation of standard reference material, i.e. SiO_2 and W. Calibration of the parameters will be performed considering a particular functional model, which will also be applied for the characterisation.

2.1. Available area shape function models

Defining the $A_p=f(h_c; \boldsymbol{a})$ requires setting the functional form and the parameters $\boldsymbol{a}$. The functional form depends on the indenter geometry. This work focuses only on modified Berkovich indenter geometry. This is a tetrahedron with a dihedral angle of 130.55°, see Figure 2, and it is the most largely adopted in nanoindentation.

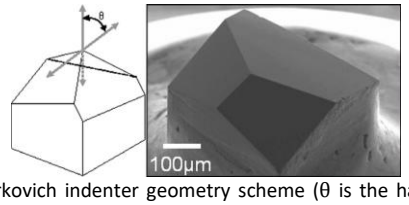

Figure 2. Berkovich indenter geometry scheme (θ is the half-dihedral angle) and a SEM image.

For an ideal indenter, it is $A_p(h_c) = 24.5 \cdot h_c^2$ and $\varepsilon = 0.75$; the modified Berkovick geometry allows having this relationship equal to the Vickers indenter. However, blunt tips and geometrical errors induce deviation from nominal geometry. These are negligible in macroscale but introduce significant errors at micro- and nano-scale. These errors must be catered for in the area shape function and they can be described by considering a more generic quadratic function. In that, several alternatives are available according to literature [4], which are reported in Table 1. Model #1 and #4 are the most complete. Although they should allow better fitting flexibility, they are scarcely adopted in literature due to their complexity. Model #2 and #5 are truncated versions of the former to improve their usability, and they are often preferred. Last, Model #3 and #6 are alternatives to the truncated versions and cater for possible small flat regions at the tip. Models #4 to #6 differ from the first three, for they hold fixed the parameter of the quadratic term to the ideal value of 24.5. This parameter is linked to the dihedral angle, and holding it fixed nominally allows extending the calibration validity range [4]. Additionally, the standard allows the adoption of a spline function, which may improve calibration performances. However, it does not allow simple management of uncertainty evaluation, which is why spline models will not be considered in the present work [6].

Table 1. Functional form of the models describing the projected area for a Berkovich indenter considered in the comparison.

#	Model Equation
1	$A_p(h) = a_8h^2 + a_7h + a_6h^{1/2} + a_5h^{1/4} + \cdots + a_0h^{1/128}$
2	$A_p(h) = a_2h^2 + a_1h + a_0h^{1/2}$
3	$A_p(h) = a_2h^2 + a_1h + a_0$
4	$A_p(h) = 24.5h^2 + a_7h + a_6h^{1/2} + a_5h^{1/4} + \cdots + a_0h^{1/128}$
5	$A_p(h) = 24.5h^2 + a_1h + a_0h^{1/2}$
6	$A_p(h) = 24.5h^2 + a_1h + a_0$

2.2. Calibration of the area shape function parameters

Calibration methods of area shape function parameters is described in ISO 14577-2:2015 [5]. Although the literature showed that available standard procedures feature criticalities [3,18], and other more promising approaches have been proposed [19], this work considers the standard calibration approach to perform the comparison at the conventional state-of-the-art. In particular, standard method number 4 is applied, which proved to be the most robust, efficient, and economic [3,18]. It relies on an iterative procedure, shown in Figure 3 and detailed elsewhere [5,18–20], that calibrates both $\boldsymbol{a}$ and C_f and requires performing replicated indentations at different loads on two standard materials, e.g. SiO_2 and W.

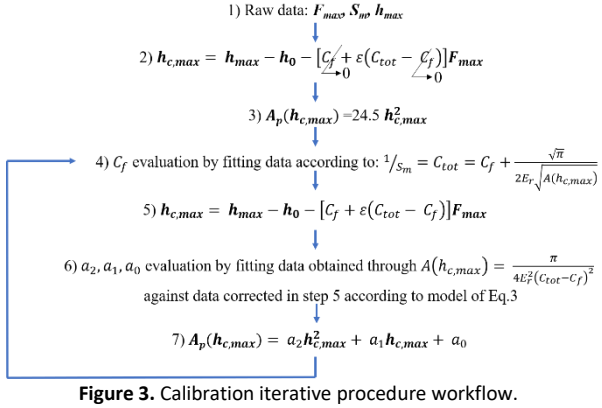

Figure 3. Calibration iterative procedure workflow.

2.3. Experimental set-up

Tests performed during the last CIRP interlaboratory comparison [21] at Oklahoma State University were considered to exploit a robust dataset. It features ten replicated indentations at four different loads, i.e. {0.5, 1, 5, 10} mN, performed on calibrated SiO_2 and W samples, whose properties are reported in Table 2. Tests were performed on a Hysitron TriboScope (resolution and noise floor of the force-displacement transducer of 1 nN and 75 nN and 0.006 nm and 0.2 nm) equipped with diamond modified Berkovich indenter (E_i = 1140

GPa, ν_i = 0.07). Results will be provided in terms E_{IT} of both materials. Characterisation in terms of H_{IT} is disregarded as it is highly dependent on area shape function and independent techniques to calibrate samples are not available. Therefore, the comparison with a calibrated value might present systematic error induced by different area shape function functional form choices in the sample calibration and the characterisation, which might overshadow the comparison at hand. This issue is not present in the case of Young's modulus as samples are typically calibrated by pulse-echo ultrasonic method [15].

Table 2. Calibrated materials characteristics with expanded uncertainty at 95% confidence level.

Material	Calibration	E / GPa	ν
SiO_2	NPL	73.3 ± 0.6	0.161 ± 0.003
W	NPL	413.0 ± 2.8	0.281 ± 0.003

2.4. Uncertainty evaluation

The effect of the functional form of the A_p is assessed on the indentation modulus E_{IT}, within a metrological framework, i.e. considering accuracy with respect to calibrated value and precision. Both require evaluating the measurement uncertainty to provide a metrologically consistent comparison. Law of uncertainty propagation according to GUM framework is applied:

$$U(y) = k \cdot u(y(\boldsymbol{x})) = k \sqrt{\sum_i \left(\frac{\partial y(\boldsymbol{x})}{\partial x_i}\right)^2 u(x_i)^2} \qquad (4),$$

where k is the coverage factor, here taken equal to 2 approximating a 95% confidence interval and $y(\boldsymbol{x})$ the generic function of Eq. 3 [22]. The standard uncertainty of the input, $u(x_i)$, are, for the force-displacement transducer, type A contribution for the repeatability and type B for the resolution (uniform distribution is considered). Indenter material mechanical properties variability is propagated as a type B contribution associated with a uniform distribution. As far as the other inputs are concerned, $u(A_p)$ and $u(S)$ are type A contributions, and their standard uncertainty is estimated including the effect of calibration. Measurement uncertainty of calibrated $\boldsymbol{a}$ and C_f includes several influence factors, reported in Figure 4 [18,19].

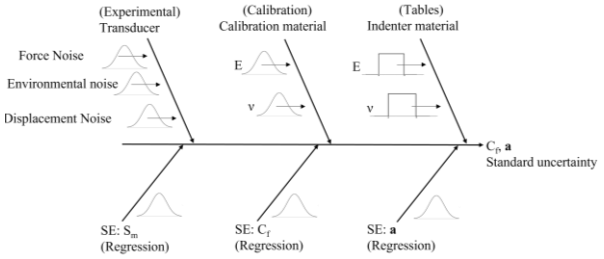

Figure 4. Ishikawa diagram of influencing factors of standard calibration methods.

However, because of the iterative nature of the calibration procedure, their evaluation from closed-form uncertainty propagation according to Eq. 4 is not possible [18,19], and simulative approaches must be resorted to. Literature has applied Monte Carlo simulation [18,19]. However, this approach disregards the effect of correlation between the force and the displacement, inherent with the IC ($F(h)$). This work proposes a bootstrap approach [23]. This, being non-parametric, does not require performing non-trivial hypotheses on the distribution of influence factors and can include effect of correlation. The empirical dataset consists of J=10 replicated indentation curves at I=4 loads; each IC contains B=8000 points. Therefore, the inputs result in pairs of F and h, both in $\mathbb{R}^{B,J,I}$. The Bootstrap samples will be sets of $I{\cdot}J$ resampled curves. Each of them, to cater for the input correlation, i.e. $F(h)$, at the b-th point, $b \in \{1,\dots,B\}$, at the i-th load, will resample the b-th point of the IC from the sample of the J observations of this point: $F(h) \in \mathbb{R}^{b,\cdot,i}$. In so doing, per each load, a maximum of J^B replicated curves may results. This number is the upper boundary of possible independent bootstrap samples that can be extracted, i.e. the number of possible calibrations and hence of evaluation of calibrated parameters that can be performed; here 11,000 datasets, i.e. bootstrap samples, are generated [23,24]. Each of those is exploited to perform a calibration, where other required quantities needed but not empirically measured, e.g. E and ν, are extracted from associated distribution, as formerly discussed. With statistical modelling of the simulative method according to the ANOVA approach [3], the resulting calibrated parameters' standard deviations are considered the related standard uncertainties, which can be propagated according to Eq. 4 to obtain the measurement uncertainty of the mechanical characterisation.

3. Results and Discussion

Results are shown in terms of indentation modulus, E_{IT}. Mechanical properties will be evaluated based on average values of the maximum force and displacement at the four considered loads. The results will be compared with the values from the calibration certificate, reported in Table 2.

Figure 5(a) shows the results of the propagation of uncertainty of calibrated parameters estimated by bootstrap sampling on the characterised quantity. As it can be noticed, models #2 and #3 (shown in Table 1) are more accurate and precise (the relative expanded uncertainty is 20% and 10%, respectively) with respect to their counterpart models #5 and #6. This is inherent in the mathematical model. In fact, by constraining one parameter, i.e. the coefficient of the h^2 term, the model is less flexible, and the gain of 1 degree of freedom to estimate the errors cannot compensate for this. Moreover, considering different mathematical models with the same number of parameters to be estimated, the model with the constant term appears to be the most accurate and precise, i.e. model #3 with respect to #2, and similarly #6 with respect to #5, see Figure 5(b). This suggests that even in the case of a tip without macroscopic errors the simplified model is suitable. The magnified views in Figure 5(b) and Figure 6(b) allow more insights on accuracy. Models #5 and #6 show sever bias at low loads (up to 50%), which is negligible, i.e. smaller than 4% and 1% respectively, for models #2 and #3. Moreover, the poorer metrological performances of models #5 and #6 pose some questions on the actual applicability of the models outside the calibration range, which is the nominal scope of their introduction [4]. In fact, within the calibration range, they result in a relative expanded uncertainty greater than 200% and in excess of 100%, respectively for model #5 and #6. Models #1 and #4 result in poor parameters estimation, i.e. often with p-values greater than 5%, and a significant systematic error in the mechanical characterisation as high as hundreds of gigapascals. Consequently, the associated uncertainty is very high and hinders effective graphical comparisons of the results, for which they are not shown. This suggests that although models #1 and #4 are potentially very detailed, the complexity in their usage may not be efficient, and spline functions might be preferred instead. Similar results are obtained considering the characterisation of tungsten. Figure 6 shows results related to models #2 and #3. Consistently with results obtained in the SiO_2 case, models #1 and #4 introduce systematic differences, and models #5 and #6 are too dispersed. The greater variability of the results typical of tungsten [19,21] worsens the results of models #5 and #6, leading to an expanded uncertainty that

hinders graphical comparison; thus, related results are not shown in Figure 6. Similar to the SiO_2 case, models #2 and #3 are the most accurate and precise, with a relative expanded uncertainty of 50% and 20%, respectively. In terms of accuracy, the models #2 and #3 present a relative bias of 6% and 3%.

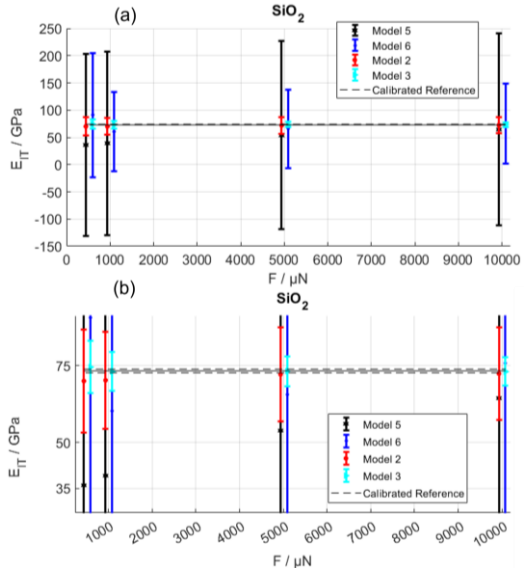

Figure 5. Comparison of characterisation of fused silica (SiO_2) indentation modulus E_{IT}; models #1 and #4 (shown in Table 1) are unreported for they introduce a significant systematic difference. (b) is a magnified view.

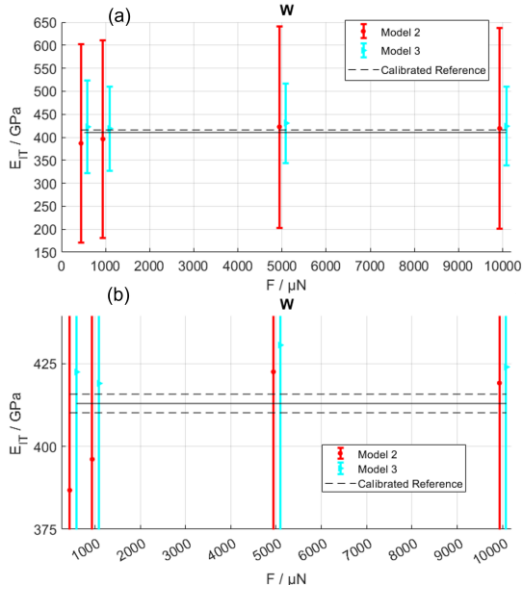

Figure 6. Comparison of characterisation of tungsten (W) indentation modulus E_{IT}; only models #2 and #3 (shown in Table 1) are reported, for the others introduce a significant systematic difference or are too dispersed. (b) is a magnified view.

4. Conclusions

This work addressed the non-trivial choice of area shape function functional form for nanoindentation. Although the literature presented some practical suggestions, a metrological comparison was missing and is proposed by this work. The work proposes a simulative non-parametric method to propagate measurement uncertainty in calibrating relevant parameters and achieve the results. The results show that models that are scarcely adopted in literature because of their greater complexity, i.e. models #1 and #4 (shown in Table 1), also present significant accuracy errors. Truncated and simplified models, i.e. model #2 and #3, feature the best accuracy and precision. Last, models that are introduced to allow extension of the calibration validity outside the range of forces actually calibrated, i.e. models #5 and #6, feature poor precision even within the calibration range.

Estimating accurately and precisely the projected area of contact is essential in nanoindentation. The present work results add valuable information to practical guidelines available in literature to choose the area shape function model while ensuring metrological performances.

Future work will consider the introduction of traceability in the calibration by comparing the area shape function obtained with independent and directly traceable methods, i.e. indentation tip measurement by AFM. Although unpractical, this will add further robustness to the analysis. Moreover, the proposed bootstrap method to evaluate measurement uncertainty, may be exploited to allow propagating the uncertainty in difficult-to-handle models, e.g. spline. Last, obtained results on different materials suggest that further research on reference materials for calibration and indirect verification is necessary in the future to reduce measurement uncertainty.

Acknowledgements

Funding by "Ministero dell'Istruzione, dell'Università e della Ricerca". Award "TESUN- 83486178370409 finanziamento dipartimenti di eccellenza CAP. 1694 TIT. 232 ART. 6"

References

[1] Lucca D A, Herrmann K, Klopfstein M J 2010 *CIRP Ann. – Manuf. Technol.* **59**:803–19.

[2] Oliver W C, Pharr G M 1992 *J. Mater. Res.* **7**:1564–83.

[3] Galetto M, Maculotti G, Genta G, Barbato G, Levi R 2019 *Nanomanuf. Metrol.* **2**(2):91-99.

[4] Oliver W C, Pharr G M 2004 *J. Mater. Res* **19**:3–20.

[5] ISO 14577-2:2015 Metallic materials-Instrumented indentation test for hardness and materials parameters-Part 2: Verification and calibration of testing machines. ISO, Genève.

[6] ISO 14577-1:2015 Metallic materials-Instrumented indentation test for hardness and materials parameters - Part 1: Test method. ISO, Genève.

[7] Herbert E G, Pharr G M, Oliver W C, Lucas B N, Hay J L 2001 *Thin Solid Films* **399**:331–335.

[8] Sebastiani M, Bemporad E, Carassiti F, Schwarzer N 2011 *Philos. Mag.* **91**:1121–1136.

[9] Roa J J, Sudharshan Phani P, Oliver W C, Llanes L 2018 *Int. J. Refract. Met. Hard. Mater.* **75**:211–217.

[10] Maculotti G, Genta G, Lorusso M, Galetto M 2019 *Key Eng. Mater.* **813**:171–177.

[11] Hou X, Jennett N M, Parlinska-Wojtan M 2013 *J. Phys. D Appl. Phys.* **46**:265301.

[12] Puchi-Cabrera E S, Staia M H, Iost A 2015 *Thin Solid Films* **578**:53–62.

[13] Renzelli M, Mughal M Z, Sebastiani M, Bemporad E 2016 *Mater. Des.* **112**:162–71.

[14] Genta G, Maculotti G, Barbato G, Levi R, Galetto M 2018 *Proc. CIRP* **78**:208–212.

[15] Maculotti G, Genta G, Lorusso M, Pavese M, Ugues D, Galetto M 2019 *Nanomanuf. Metrol.* **2**(1):16-25.

[16] Sneddon I N 1965 *Int. J. Eng. Sci.* **3**:47–57.

[17] Barbato G, Genta G, Cagliero R, Galetto M, Klopfstein M J, Lucca D A, Levi R 2017 *CIRP Ann. – Manuf. Technol.* **66**:495–498.

[18] Maculotti G, Genta G, Galetto M 2020 *Conf. Proc. of 20th Int. Conf. Exhib. EUSPEN*: 2–5.

[19] Galetto M, Genta G, Maculotti G 2020 *CIRP Ann.* **69**:429–432.

[20] Herrmann K, Jennet N M, Wegener W, Meneve J, Hasche K, Seeman R 2000 *Thin Solid Films* **377–378**:394–400.

[21] Herrmann K, Lucca D A, Klopfstein M J, Menelao F 2010 *Metrol.* **47**:S50-S58.

[22] JCGM 100:2008 Evaluation of measurement data - Guide to the expression of uncertainty in measurement (GUM). JCGM, Sèvres.

[23] Efron B 1979 *Ann. Stat.* **7**:1–26.

[24] JCGM 101:2008 Evaluation of measurement data - Supplement 1 to the "GUM" - Propagation of distributions using a Monte Carlo method. JCGM, Sèvres.